RSC Advances

PAPER

View Article Online
View Journal | View Issue

Cite this: *RSC Adv.*, 2020, **10**, 21028

Tunable and switchable nanoparticle separation with thermo-responsive track-etched membranes prepared by controlled surface-initiated polymerization of poly(*N*-isopropylacrylamide)†

Kevin Daumann,[ab] Sven Frost[ab] and Mathias Ulbricht *[ab]

This work describes how the control of grafting density and grafted chain length of a thermo-responsive polymer in membrane pores can be utilized to tune the pore size and the switchability of size-based selectivity in the ultrafiltration range. Using a previously established methodology for controlled synthesis, surface-initiated atom transfer polymerization (ATRP) of poly(*N*-isopropylacrylamide) (PNIPAAm) to the pore walls of poly(ethylene terephthalate) track-etched membranes with experimentally determined pore diameters of 35 nm (PET30) and 110 nm (PET80) is performed. Characterization in this study is mainly done with filtration experiments, making use of the well-defined pore structure of the base membranes. It is demonstrated that both the gravimetrically determined degree of functionalization and the effective pore size determined from water permeability are a linear function of ATRP time. For the grafted PET30 membranes, it is shown that the rejection of lysozyme (diameter ~ 4 nm) can be switched between 99% at 23 °C and 65% at 45 °C for the membrane with the highest degree of functionalization. For the grafted PET80 membranes, it is found that two different types of membranes can be obtained. Membranes with long grafted chains at low grafting density show very large changes of water permeability as a function of temperature (effective pore size switching ratio of up to 10) and, for example, rejection for 20 nm silica particles of 95% and 23% at 23 °C and 45 °C, respectively. Membranes with PNIPAAm at high grafting density show much lower switching ratios (as low as 1.4, for long enough grafted chains). Effective pore size and thermo-responsive change of pore size can therefore be tuned by the combination of both synthesis parameters, initiator density and ATRP time. The switchable thermo-responsive separation of two colloids with a tailored membrane is demonstrated for mixtures of bovine serum albumin (BSA; ~7 nm) and silica nanoparticles (20 nm); at 23 °C silica is completely rejected and only BSA is in the permeate; at 40 °C both colloids permeate through the membrane.

Received 16th April 2020
Accepted 26th May 2020

DOI: 10.1039/d0ra03418e

rsc.li/rsc-advances

1. Introduction

Stimuli-responsive membranes are becoming increasingly popular due to their dynamic barrier structure.[1] With a view of the resulting separation properties, one well-designed and prepared membrane can act like several different membranes, just controlled by internal or external stimulation of the system. Typical stimuli are changes of chemical or physical quantities, for example pH and ionic strengths of the feed, or feed/membrane temperature and external magnetic fields.[2–4] A substantial and reversible alteration of the barrier properties as a consequence of an external stimulation with low intensity is of high interest for mass separation and other possible applications like triggered release of drugs. Numerous examples for such membranes have been described in the literature. However, in the majority of the studies just the change of liquid flux had been reported while significant and reversible changes of transport selectivity of specific target substances or even the switchability of mixture separation selectivity are less frequently achieved.

The focus of this work is on thermo-responsive ultrafiltration membranes. One preferred strategy to obtain those is the functionalization of a porous base membrane with a thermo-responsive polymer, either by grafting polymer chains to the membrane surface or by pore-filling with a polymeric hydrogel.[3] The classical example, which had been very well studied, is poly(*N*-isopropylacrylamide) (PNIPAAm), which exhibits a lower critical solution temperature (LCST) at 32 °C in water.[5] This

[a]*Lehrstuhl für Technische Chemie II, Universität Duisburg-Essen, Universitätsstr. 7, 45141 Essen, Germany. E-mail: mathias.ulbricht@uni-essen.de*

[b]*Center for Nanointegration Duisburg-Essen (CENIDE), 47057 Duisburg, Germany*

† Electronic supplementary information (ESI) available. See DOI: 10.1039/d0ra03418e

amphiphilic polymer is below its LCST in a swollen state due to dominating hydration of chain segments *via* formation of hydrogen bonds; above the LCST the polymer is in a collapsed state because the hydrophobic character of chain segments dominates. The intrinsic rate of this transition is fast; the response to a sudden increase or decrease of temperature above/below LCST occurs within milliseconds for grafted layers of about 100 nm thickness.[6] The feasibility of utilizing the switchability of PNIPAAm as active component in porous membranes for mass separation has been demonstrated by the temperature controlled adsorption/desorption of relatively hydrophobic substances under flow-through conditions,[7,8] but in such cases the membrane is used as an adsorber which requires regeneration once binding capacity is saturated. In two other papers on membranes with pore-grafted PNIPAAm, the change of protein rejection with temperature in single solute experiments was reported, but the effects were very small.[9,10] Utilizing the switchable (effective) pore size as function of temperature with integrated PNIPAAm to achieve responsive size separation of colloidal particles has been shown by Zhu *et al.*,[11] who had prepared a PNIPAAm/polysulfone blend membrane and demonstrated the switchable selectivity for separation of gold and silver nanoparticles, and by Frost and Ulbricht[12] with well-defined capillary pore membranes for switchable permeation of silica nanoparticles of different size (see below).

Poly(ethylene terephthalate) (PET) track-etched membranes (TEM) with well-defined capillary pore structure had been established as versatile model system for stimuli-responsive membranes in general in order to establish functionalization procedures and to obtain reliable quantitative information about the interplay between base membrane pore structure and functional polymer.[3,12–15] For thermo-responsive membranes it had previously been reported that not only the flux, but also the separation selectivity in the ultrafiltration can be switched by changes of temperature when porous base membranes are functionalized with PNIPAAm. This has been achieved by pore-filling, so that the mesh size of the hydrogel acts as molecular sieving medium at low temperature while the heterogeneously collapsed polymer leads to much larger effective pore size at high temperature.[16] The alternative was controlled surface initiated graft copolymerization of PNIPAAm from the pore walls of PET TEM with a mean pore diameter of 110 nm, so that the grafted layer thickness could be tuned by synthesis condition and its thermo-responsive swelling/deswelling transition could be utilized to switch the effective pore diameter in the range of 20 to 100 nm.[12] In the latter study the adaptation of previously established controlled surface-initiated atom transfer radical polymerization (SI-ATRP) (*cf.* ref. 14) to the relatively small base membrane pores size had been a crucial aspect. Hence, the effective pore diameters at temperatures below and above the LCST were clearly distinguishable and the switchable selective permeation of silica nanoparticles with sizes of 35 nm or 21 nm was demonstrated.[12]

The present work is a significant extension of this previous study in three important aspects. First of all, the controlled grafting in terms of membrane preparation *via* SI-ATRP has been extended to smaller base membrane pore size (~35 nm), so that membranes with effective pore sizes below 10 nm have been obtained as demonstrated by the switchable size-separation of the model protein lysozyme (diameter about 4 nm). Secondly, the initiator group density on the surface of PET TEM (110 nm) has been varied with the aim to vary the grafting density of PNIPAAm chains (in analogy to the work with PET TEM of much larger pore size and another grafted copolymer[17]). At high grafting densities, *i.e.* in the "brush" regime the mutual repulsion between grafted chains lead them to stretch away from the surface in both, the swollen and collapsed state.[18] Thus, PNIPAAm layers with the same grafted chain length, but lower grafting density, should lead to larger switching ratios.[19] In this "mushroom" regime the mutual interactions between adjacent chains do not prevent complete collapse onto the surface; hence, when this control of grafting density can be implemented for SI-ATRP of PNIPAAm in PET TEM, the difference between effective pore diameter below and above LCST should be larger for lower grafting density (see Scheme 1).[20] Such higher switching ratios can be used for more challenging particle filtrations which is the third focus of this work. Silica nanoparticles with an average size of 20 nm as well as the protein bovine serum albumin (BSA) with an average size of 7 nm, individually or in a mixture, were used in ultrafiltration using membranes prepared under different conditions and at temperatures below and above LCST.

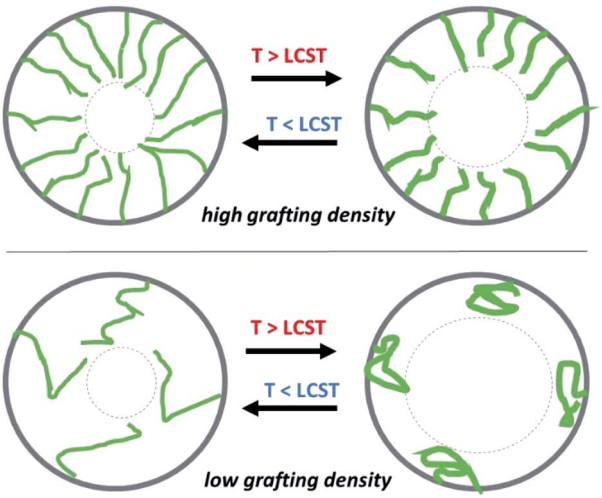

Scheme 1 Schematic visualization of pores with a grafted thermo-responsive polymer at high and low grafting densities but about same chain length, showing that the effective pore diameter for unhindered flow through the pore changes to larger extent upon a change of temperature for low grafting density, *i.e.* a larger switching ratio is expected for isoporous membranes at low grafting density.

2. Experimental section

2.1 Materials

Poly(ethylene terephthalate) track-etched membranes with a thickness of 8 μm and a nominal pore diameter of 80 (named PET80) and 30 nm (named PET30) were purchased from Oxyphen AG, Wetzikon (Switzerland). Actual mean pore diameters

determined by gas flow/pore dewetting permporometry were 111 ± 2 and 35 ± 1 nm for PET80 and PET30, respectively.[12] Pure water from a MilliQ2 water purification system (Millipore, Eschborn, Germany) was used for all experiments. *N*,*N*′-Diisopropylcarbodiimide (99%) and $CuBr_2$ (>99%) were obtained from Acros Organics. Acetonitrile (99.99%) was also from Acros Organics and dried by adding 10 g of boron trioxide (B_2O_3, 99%) to a volume of 250 mL and refluxing for 2 h. *N*-Isopropylacrylamide (NIPAAm, 99%) from Acros Organics was recrystallized twice from *n*-hexane (99.9%, from AnalR Normapur). Dimethylformamide (DMF; 99.8%) and sodium chloride (99.7%) were from AnalR Normapur. Methanol (99.99%) and sulfuric acid (98%) were obtained from Fisher Scientific. Ethanolamine (>99%), *N*,*N*,*N*′,*N*″,*N*″-pentamethyl diethylenetriamine (PMDETA, >98%), triethylamine (>99.5%), 4-dimethylaminopyridine (≥98%), potassium permanganate (≥99%) and lysozyme were purchased from Fluka. *N*-Hydroxybenzotriazole (>97%), α-bromoisobutyryl bromide (98%), propionyl bromide (97%), CuCl (99.995%), $CuCl_2$ (99.99%), hydrochloric acid (≥37%) and HS-40 colloidal silica (40 wt%, dispersion in water) were received from Sigma Aldrich. 1 mol L^{-1} sodium hydroxide standard solutions were from AVS Titrinorm and used as received to adjust the pH of the nanoparticle dispersions. Bovine serum albumin (BSA, 100%) was obtained from Gerbu Biotechnik GmbH. Tris[2-(dimethylamino)ethyl]amine (Me_6TREN) was synthesized according to literature.[21]

2.2 Variation of initiator group density

The as-received membranes were washed in methanol for 1 h and subsequently dried at 55 °C for 1 h. The following "oxidative hydrolysis", using an acidic solution of potassium permanganate to maximize density of carboxylic acid groups and their conversion *via* carbodiimide-activated amidation with ethanolamine to obtain a high density of hydroxyl groups were performed as described before.[12,14,15] The subsequent immobilization of the ATRP initiator was done by esterification of the surface hydroxyl groups with α-bromoisobutyryl bromide. The density of ATRP initiator groups on the membrane surface depends on the molar ratio of α-bromoisobutyryl bromide, the reagent with active initiator group and propionyl bromide, the analogous reagent but without initiator group.[14,17] If the fraction of propionyl bromide is zero, the membrane surface will be completely covered by initiator groups as reported before, corresponding to a density of ~1 group per nm^2.[12,14] For modification the membranes were put in 100 mL of a solution of 5 mmol L^{-1} 4-(*N*′,*N*′-dimethylamino)pyridine, 100 mmol L^{-1} triethylamine and 81 mmol L^{-1} α-bromoisobutyryl bromide/propionyl bromide with the desired fraction (100, 50 or 10% α-bromoisobutyryl bromide) in dry acetonitrile for 2 h. Afterwards the membrane samples were washed twice with either acetonitrile and methanol and subsequently dried and cut in 44 mm diameter disks and weighed with a GENIUS balance (accuracy: ± 10 μg) from Sartorius (Germany).

2.3 SI-ATRP

ATRP was performed with DMF as solvent at room temperature. The molar ratio between monomer and the components of the catalyst system used for all experiments was [NIPAAm] : [Me_6-TREN] : [CuCl] : [$CuCl_2$] = [120] : [1.5] : [1] : [0.1]. The concentration of NIPAAm was 1 mol L^{-1} for functionalization of PET80 membranes and 0.5 mol L^{-1} for functionalization of PET30 membranes. After the predetermined reaction time between 20 min and 3 h, the reaction was stopped by adding a solution containing $CuBr_2$ and PMDETA in DMF. The degree of graft functionalization (DG) which was calculated according to eqn (1):

$$\mathrm{DG} = (m_{\mathrm{gr}} - m_0)/A \quad (1)$$

where m_0 is the membrane weight after initiator immobilization, m_{gr} is the membrane weight after grafting (*cf.* Section 2.2), and A is the specific surface area of the used 44 mm diameter membrane sample (specific surface area determined by nitrogen adsorption and BET analysis). A detailed synthesis procedure can be found in ESI.†

2.4 Water flux measurement and estimation of hydrodynamic pore diameter

The permeability of the membranes was measured with a 0.01 mol L^{-1} NaCl solution in deionized water at pH 10 using a 50 mL Amicon cell (Millipore, MA, USA), which was connected to a pressure reservoir operated with argon for adjustment of the transmembrane pressure. For both unmodified and modified membranes the water flux, J_w, had been determined three times. The permeate was collected in a 50 mL beaker within 5 min and the amount of water was determined gravimetrically. Pure water permeability, P, was calculated according to eqn (2):

$$P = J_w/\Delta P = V_{\mathrm{membrane}}/(A_M \Delta t \Delta P) \quad (2)$$

V_{membrane} is the permeate volume flowing through the whole membrane, A_M is the geometric (outer) surface area of the membrane, Δt is the measuring time interval, and ΔP is the applied transmembrane pressure.

Hagen–Poiseuille's law was used to determine the hydrodynamic pore diameters of the modified membranes. Eqn (3) is valid for a single pore:

$$V_{\mathrm{pore}}/\Delta t = \pi \Delta P r^4/(8\eta L) \quad (3)$$

V_{pore} is the permeate volume flowing through a single capillary pore, r is the hydrodynamic pore radius, η is the viscosity of water and L is the membrane thickness, *i.e.*, the length of one capillary pore. Considering all the membrane pores and using the pore diameter instead of the radius, eqn (3) can be transformed to eqn (4):

$$V_{\mathrm{membrane}}/\Delta t = N_p A_M \pi \Delta P d^4/(128\eta L) \quad (4)$$

N_P is the pore density, and d is the hydrodynamic pore diameter. The pore density was calculated by measuring the water flux of the unmodified membranes and using the mean pore size of this membrane, which was obtained from gas flow/pore dewetting permporometry (*cf.* Section 2.1). It is assumed that the pore density remains unchanged after the membrane modification. Consequently, the hydrodynamic pore diameter

for the modified membranes can be obtained using eqn (4); the hydrodynamic layer thickness on the pore wall l_h is obtained as difference of the respective hydrodynamic pore radii for unmodified and modified membranes.

2.5 Silica nanoparticle ultrafiltration

The as-received HS-40 silica nanoparticle (NP) dispersion was diluted with a 0.01 mol L^{-1} sodium chloride solution to a concentration of 0.5 g L^{-1} followed by an ultrasonic treatment (15 min, 100% intensity, Elma GmbH, Singen, Germany). To adjust the pH of the dispersion an adequate amount of 1 mol L^{-1} sodium hydroxide standard solution was added. The feed volume for each filtration was 20 mL. 15 mL of it were filtered through the membrane and collected as permeate. To obtain a flux profile the permeate weight was determined gravimetrically in certain time intervals. The NP concentration in the feed and permeate was determined photometrically as described before.[12] The UV-vis fluorescence spectrophotometer Cary (Varian) was used at $\lambda_{ex} = 278$ nm and $\lambda_{em} = 288$ nm; a linear calibration curve was obtained for at least six different dilutions in the range between 15 and 500 mg L^{-1}. The colloid rejection was then calculated according to eqn (5):

$$R = (1 - c_P/c_F)100\% \quad (5)$$

R is the rejection, c_P and c_F are the concentrations of test colloid in permeate and feed, respectively. For each filtration above and below the LCST of PNIPAAm a new membrane was used. More details about filtration conditions will be given in Section 3.3.

2.6 Protein ultrafiltration

50 μg of BSA or lysozyme was dissolved in a 1/15 mol L^{-1} phosphate buffer solution with a pH of 8 to yield 100 mL. The feed volume for each filtration was 20 mL of which 15 mL were filtered through the membrane and collected as permeate. To obtain the flux profiles, permeate was weighed in short time intervals. The concentration of BSA in feed and permeate was determined using the BCA assay by photometric measurements with a microplate reader at a wavelength of 280 nm using a calibration curve. Permeates were analyzed with 3 samples for each filtration. Rejection was calculated with eqn (5). More details about filtration conditions will be given in Section 3.3. For size determination of proteins in solution dynamic light scattering (DLS) using the instrument StabiSizer PMX 200 from ParticleMetrix was measured (see ESI, Fig. S1 and S2†).

2.7 Ultrafiltration separation of BSA/silica NP mixtures

HS-40 silica NP dispersion ($c = 0.25$ mol L^{-1}) as well as BSA ($c = 0.25$ mol L^{-1}) were combined in a phosphate buffer solution with a pH of 8 to yield 20 mL. The formation of agglomerates was minimized since silica NP as well as BSA are negatively charged at pH 8. Filtration procedure was similar to previously described particle filtrations. Selectivity was analyzed by DLS (*cf.* Section 2.6) and compared to single particle and mixed particle dispersions/solutions. A shift to lower particle sizes indicates a selective transport of BSA through the membrane while rejecting silica particles.

3. Results and discussion

3.1 Synthesis of PET30-*g*-PNIPAAm membranes and their thermo-responsive filtration properties

The TE membrane (PET30) used here had an experimentally determined pore diameter of 35 nm. Pre-functionalization and ATRP initiator immobilization on the PET30 membrane pore surface had been performed using the same conditions as established for PET TE membranes with larger pore size. Because the pores are obtained with the same base polymer under the same track-etching conditions and considering the small size of reactants and relatively long reaction times (between 20 and 120 min), it is assumed that the density of functional groups on the surface is the same for all pore sizes. That had been proven experimentally in earlier studies for PET TEM with larger pore size (most specifically regarding the contents of this study by X-ray photoelectron spectroscopy (XPS) analysis of Br density on ATRP initiator-functionalized PET TE

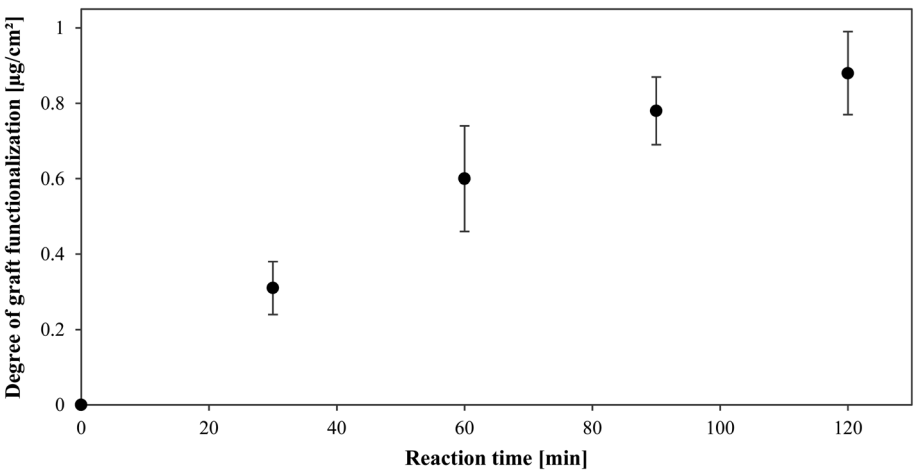

Fig. 1 Degree of grafting (DG) as function of reaction time for SI-ATRP toward PET30-*g*-PNIPAAm membranes.

membranes with nominal pore diameter of 400, 1000 and 3000 nm).[17] However, considering the challenge to maintain constant conditions for a controlled polymerization of the entire pore surface at reduced pore diameter (from 110 to 35 nm), *i.e.* increased aspect ratio (with 8 μm membrane thickness in both cases increased from 73 to 229), SI-ATRP with the PET30 membrane has been performed with a monomer (NIPAAm) concentration of 0.5 mol L^{-1}, which is only half of the monomer concentration used for PET80 membranes. The concentration of the catalyst system was also reduced accordingly (*cf.* Section 2.3). The results in Fig. 1 show that an almost linear growth of the degree of functionalization with reaction time was obtained. The initial polymerization rate (within the first 20 min) was lower (0.017 μg cm^{-2} min^{-1}) compared to the SI-ATRP experiment with PET80 at higher NIPAAm concentration (0.024 μg cm^{-2} min^{-1}). Additionally a more pronounced decrease in overall grafting rate compared to PET80 could be observed (*cf.*[12] and Section 3.2).

The effective hydrodynamic pore diameters which had been estimated as described in Section 2.4 are shown in Fig. 2. A systematic decrease with polymerization time as well as a very pronounced dependency on temperature was observed. Qualitatively this is similar to what had been found earlier for the analogous functionalization of PET80 membranes.[12] The estimated pore diameter at 23 °C was 7 nm after a reaction time of 120 min and the analysis of water flux indicated that the pore diameter of this membrane could be increased to about 20 nm by increasing the temperature to 45 °C.

The rejection of the model protein lysozyme was determined for unmodified and grafted membranes (Fig. 3). The DLS measurement of the lysozyme dispersion yielded in a hydrodynamic diameter of about 3–4 nm which is in good agreement with the dimensions according to its molecular structure,[22] (*cf.* ESI, Fig. S1†). The values observed for the unmodified membrane were much higher than expected based on pore and particles sizes and an increase of rejection at 45 °C was found as well. In addition to hindrance effects due to the low membrane

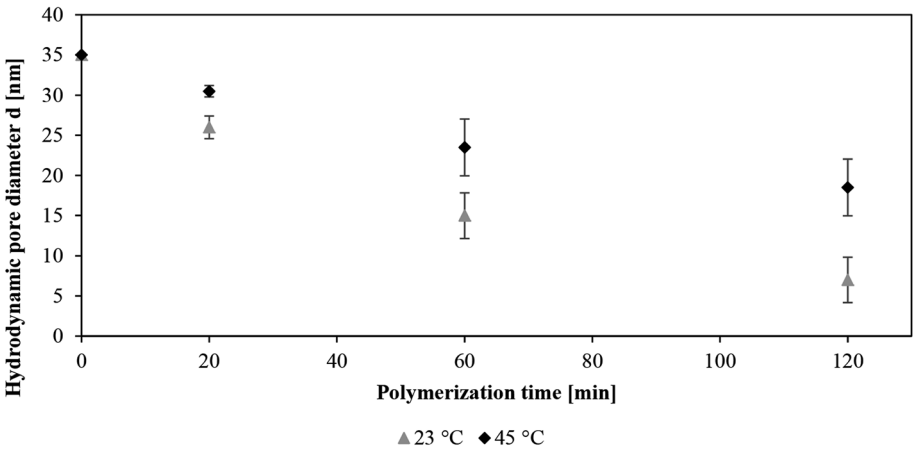

Fig. 2 Effective pore diameter of PET30-*g*-PNIPAAm membranes, determined from water permeability at two different temperatures, as function of SI-ATRP time.

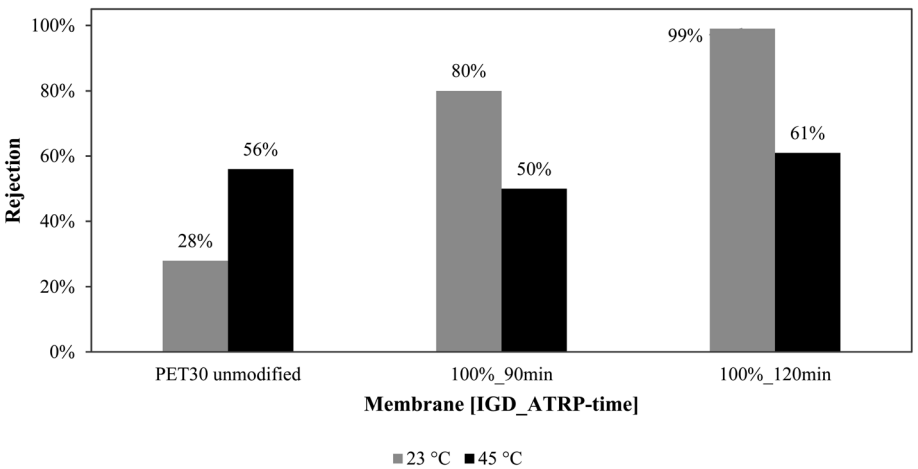

Fig. 3 Lysozyme rejection for ultrafiltrations through unmodified and PET30-*g*-PNIPAAm membranes (the relative error of data from repeated experiments was <10%).

surface porosity, partial aggregation of the protein (more pronounced at higher temperature) is another possible reason; but this was not investigated in more detail. However, for the same protein solutions significantly higher rejections, systematically increasing with SI-ATRP reaction time, were observed. Furthermore, the rejection for the grafted membranes above LCST of PNIPAAm was much lower. After a reaction time of 120 min, quantitative rejection of lysozyme was obtained at 23 °C (estimated pore size 7 nm; *cf.* Fig. 2) while rejection dropped to about 60% at 45 °C (estimated pore size 20 nm; *cf.* Fig. 2). The semi-quantitative agreement between observed size selectivity in protein ultrafiltration and calculated pore size estimates from another filtration experiment with pure water as well as the effect itself are very interesting and potentially relevant (*e.g.* for triggered protein release through such a membrane). However, it must also be mentioned that the assumptions made for the estimation of hydrodynamic pore diameter – homogeneous grafted layer (constant polymer density over thickness) with the same thickness on the entire pore surface and no flux through the grafted layer – describe the system in an idealized/simplified manner. It is known that the polymer density within real grafted layers (on planar surfaces) may decrease significantly with increasing distance from the surface due to polydispersity, *i.e.* different chain lengths. On the other hand, the curvature of the surface in the pore may have an opposite effect (and this will also depend on grafting density; *cf.* Section 3.2).[20] Finally, the density of the grafted layer will also determine whether the "no flow through" assumption (compared to convective flow of bulk water in free pore space) is really justified; such approximation will only be valid if the grafting density is high enough so that a "brush" state is reached. Considering the thermo-responsivity, the switching ratio, *i.e.* the change of grafted layer thickness upon thermal stimulation can be taken as a quantitative indicator. The values calculated from data shown in Fig. 2 are 2.5 for the membranes obtained after 20 and 60 min SI-ATRP time and 1.8 after 120 min. The reduction with increasing time, *i.e.* increasing layer thickness, indicates that an additional confinement effect lead to higher (average) polymer density in the layer. All values are within or very close to the range which is typical for the "brush" regime (switching ratio 1.5 to 2).[12,18,23]

All results demonstrate that it was possible to graft thin PNIPAAm layers at high grafting density inside the PET membrane pores with 35 nm without plugging them and with a very well-defined thermo-response. This is a strong evidence for a very well controlled membrane functionalization.

3.2 Synthesis and characterization of PET80-*g*-PNIPAAm membranes with varied initiator densities *via* SI-ATRP

The TE membrane (PET80) used here had an experimentally determined pore diameter of 110 nm. The pre-modification of PET80 membranes was performed as in previous own work,[12] with the exception of the variation of the initiator group density (IGD). Tomicki *et al.*[17] had reported that, based on XPS analysis of the ATRP initiator functionalized membrane surfaces, the analogous procedure lead to an over-proportional dilution of actually found Br-containing initiator sites on the surface compared to the stoichiometry of the reaction mixture. Results for SI-ATRP of NIPAAm on the membrane surface are shown in Fig. 4. Growth rates for degree of grafting on membrane surfaces with 100% and 50% IGD were identical within the experimental error. The decrease of IGD to 10% lead to a large reduction of degree of grafting for identical polymerization times (under identical reaction conditions). These results are in line with the assumption that the initiator groups on membranes with high IGD are not used completely to start polymerization of grafted chains. This is a well-known phenomenon in surface-initiated graft copolymerization and had been discussed in detail before;[24,25] analogous empirical results had been also already found for grafting PNIPAAm in PET TE membranes with larger pores.[12,14] Direct experimental determination of actual grafting density is very complicated and has only very rarely been performed.[13] Two assumptions are generally made. First, for higher IGD, the achieved grafting density will be limited by the actual reactivity of the polymerization system and steric hindrance, leading to the same grafting density. Second, chain growth rate will only depend on the reaction conditions (monomer and catalyst system concentrations, solvent and temperature) leading to the same growth rate irrespective IGD. For different experiments under same polymerization conditions the ratio between growth rates for degree of grafting will correspond to the ratio of polymer grafting density. Hence, grafting density would be about 60% when using 10% IGD in comparison to the maximum grafting density (achieved at 50 and 100% IDG; *cf.* Fig. 4).

Table 1 Overview on data for PET80-*g*-PNIPAAm membranes prepared at varied SI-ATRP conditions: measured water permeability *P*, as well as calculated hydrodynamic pore diameter *d* and hydrodynamic layer thickness l_h at 23 °C and 45 °C. Thermo-responsive switching ratio was calculated from l_h at 23 °C and 45 °C. All flux characterizations were performed at pH 10 and 0.01 mol L^{-1} NaCl

Membrane	DG [μg cm^{-2}]	*P*@23 °C [L (h^{-1} m^{-2} bar^{-1})]	*P*@45 °C [L (h^{-1} m^{-2} bar^{-1})]	*d*@23 °C [nm]	*d*@45 °C [nm]	l_h@23 °C [nm]	l_h@45 °C [nm]	Switching ratio
10%_60 min	0.68	700	1933	94	108	10	1	10.0
50%_60 min	0.94	403	1084	82	94	16	9	1.8
100%_60 min	0.87	363	1270	80	97	17	7	2.4
10%_180 min	0.99	99	1238	58	97	28	7	4.0
50%_180 min	1.77	9	100	32	52	41	30	1.4
100%_180 min	1.71	9	158	32	58	41	27	1.5

Table 2 Summary of membranes used for colloid ultrafiltrations with degree of graft functionalization DG (for grafted PET80 membranes), used colloids, temperature T, hydrodynamic pore diameter d determined by water permeability measurement (*cf.* Table 1), applied pressure Δp, initial flux J_0 as well as relative final flux at the end of ultrafiltration J/J_0

Membrane	DG [μg cm^{-2}]	Used colloid	T (°C)	d [nm]	Δp [mbar]	J_0 [L m^{-2} h^{-1}]	J/J_0
PET80	—	Silica	23	110	50	80	0.60
PET80	—	BSA	23	110	50	44	0.41
PET30	—	Silica	23	35	2000	60	0.65
PET30	—	BSA	23	35	500	6	0.13
50%_20 min	0.55	Silica	23	96	100	70	0.61
50%_20 min	0.58	Silica	45	108	50	78	0.61
10%_60 min	0.64	Silica	23	80	100	29	0.44
10%_60 min	0.62	Silica	45	94	50	52	0.61
50%_70 min	0.86	Silica	23	68	500	51	0.44
50%_70 min	0.86	Silica	45	96	100	53	0.65
10%_180 min	1.14	Silica	23	39	1000	19	0.34
10%_180 min	0.91	Silica	45	88	100	44	0.67
100%_120 min	1.41	BSA	23	41	1000	18	0.97
100%_120 min	1.14	BSA	40	89	100	36	0.92
50%_180 min	1.62	BSA	23	22	2000	9	0.78
50%_180 min	1.36	BSA	40	88	50	29	0.48
10%_360 min	1.32	BSA	23	26	2000	27	0.16
10%_360 min	1.14	BSA	40	84	100	30	0.29
10%_60 min	0.50	Silica + BSA	23	89	100	26	0.07
10%_60 min	0.53	Silica + BSA	40	104	50	42	0.30

That the varied IGD is indeed connected to the polymer grafting density in a strongly non-linear way can be seen from the results of water flux characterization shown in Table 1 since the switching ratios are similar for 100 and 50% IGD, but much larger for 10% IGD. In general, water permeability at 23 °C decreased with increasing degree of grafting, but for similar degree of grafting the permeability of membrane 10%_180 min was much lower than that of 50%_60 min and 100%_60 min. This could tentatively be linked to the longer polymer chains, due to longer polymerization time. However, the membranes comprising grafted layers with same chain length obtained at higher initiator and grafting density (50%_180 min and 100% _180 min) had much lower permeability. Obviously the grafting density had an additional effect, namely leading to larger layer thickness at same grafted chain length. This is due to stretched macromolecule conformations caused by mutual repulsion between neighbored chains, *i.e.*, the "brush" state. The effect of available space between the grafted chains becomes even more obvious when temperature is increased to 45 °C. According to the data polymer layers are not able to fully collapse when high IGD (50% and 100%) was used, resulting in relatively low switching ratios of 1.4 to 2.5. More free space between chains for membranes with low IGD lead to a massive increase in switching ratios, from 4.0 at high DG up to 10.0 at low DG (*cf.* Scheme 1). The consistently higher switching ratios for all three IGD with increasing polymerization time are in line with theory because the transition from loosely grafted "mushroom"-like to "brush" layers at same grafting density is promoted with increasing grafted chain length.[18] According to the criteria already evoked in Section 3.1, the membranes obtained at IGD of 50 or 100% and 180 min reaction time are clearly in the "brush" state while the membrane obtained at IDG of 10% and 60 min reaction time is clearly in the "mushroom" state. Other combinations of IGD and reaction time can be used to adjust structures in between. These differences in switching ratios, in combination with the tuning of pore size range, were in the following investigated for the ultrafiltration of silica nanoparticles and the model protein BSA (Section 3.3).

3.3 Colloid filtration

The average particle size as determined by DLS was about 20 nm for the silica nanoparticles (*cf.*[12] and below) and about 7 nm for BSA (in agreement with its structure[26]). All relevant information about the performed colloid filtrations is shown in Table 2. Unmodified membranes were included as reference. Based on insights gained in Section 3.2, membrane preparation conditions had been selected or adapted, in order to achieve most

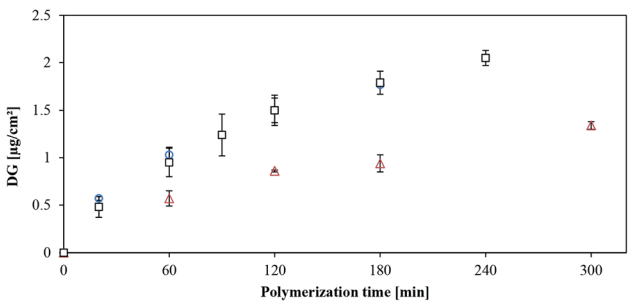

Fig. 4 Degree of functionalization in dependency of reaction time for different initiator densities, for preparation of PET80-*g*-PNIPAAm: black squares: 100% IGD; blue circles: 50% IGD; red triangles: 10% IGD.

pronounced changes of size-selectivity upon temperature change and to be able to discuss correlations of colloid rejection with estimated hydrodynamic pore sizes. Transmembrane pressure had been adapted to the membrane permeability; due to the partially blocked state of the thermo-responsive membranes at lower temperature the pressure was higher compared to the same membrane at higher temperature. BSA ultrafiltration had been done at only 40 °C, instead of 45 °C as used for water flux and silica filtration experiments, in order to avoid denaturation (stability over time at this temperature was confirmed by DLS; see Fig. S2†). The change of hydrodynamic pore size was negligible in this temperature range (40–45 °C) well above the LCST of PNIPAAm. Nevertheless, more fouling was observed for the ultrafiltrations with BSA compared to those with silica, as indicated by the lower J/J_0 values. This must also be kept in mind for the interpretation of the data, but the focus will be on observed rejections. A new membrane was used for each experiment in order to observe and discuss the effect of the membrane structure on selectivity (this is the reason for slight differences in DG of individual membranes of the same membrane type).

3.3.1 Silica nanoparticle filtration. The rejection of silica nanoparticles with 20 nm diameter for selected PET80-*g*-PNIPAAm membranes with different grafting density and chain length is shown in Fig. 5. Rejection for NP by unmodified PET80 and PET30 membranes at 23 °C was 1 and 22%, respectively. This indicates unhindered passage of the 20 nm particles through 110 nm wide pores while for the 35 nm wide pores significant hindrance effects occur.[27] The significant reduction of permeability during the filtration as seen in the J/J_0 values of 0.60 and 0.65 indicates that particle fouling may also contribute to the rejection; similar effects for other nanoparticles and other TE membranes had been observed by Lee *et al.*[28] A very low degree of grafting leads to a slight increase of hindrance, *i.e.* rejection (irrespective the still large estimated effective pore size of 96 nm), but with increase of temperature this rejection is switched off (50%_20 min). Much more interesting is the higher rejection obtained for the membrane with same IGD but longer polymerization time (50%_70 min), in combination with a very

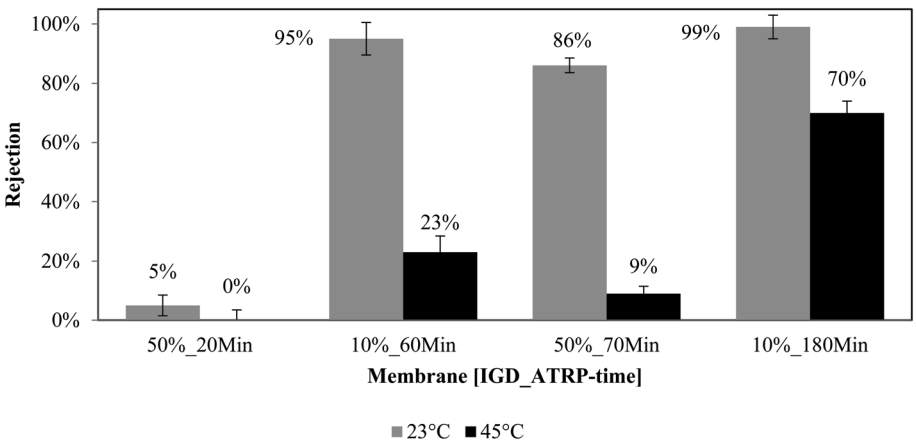

Fig. 5 Rejection of membranes for silica nanoparticles with 20 nm diameter at 23 °C as well as 45 °C and a feed concentration of 0.5 g L^{-1}. All measurements were performed with grafted PET80 membranes (the relative error of data from repeated experiments was <10%).

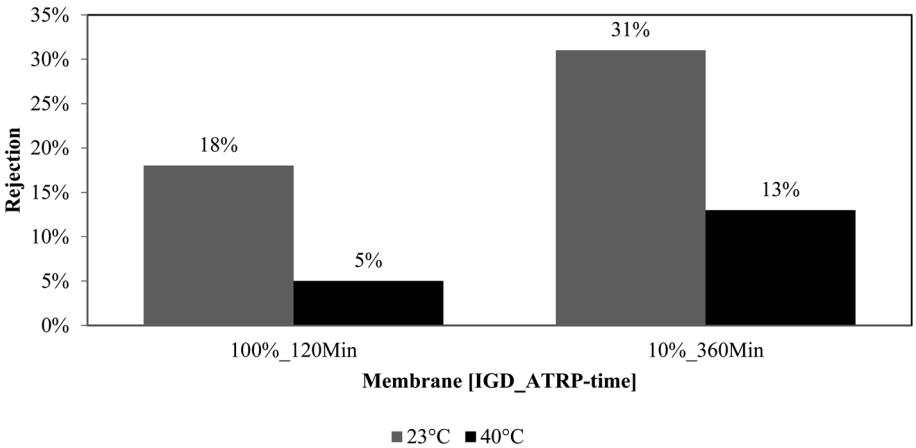

Fig. 6 Rejection of membranes for BSA at 23 °C as well as 40 °C and a feed concentration of 0.5 g L^{-1} in phosphate buffer (pH 8; the relative error of data from repeated experiments was <10%).

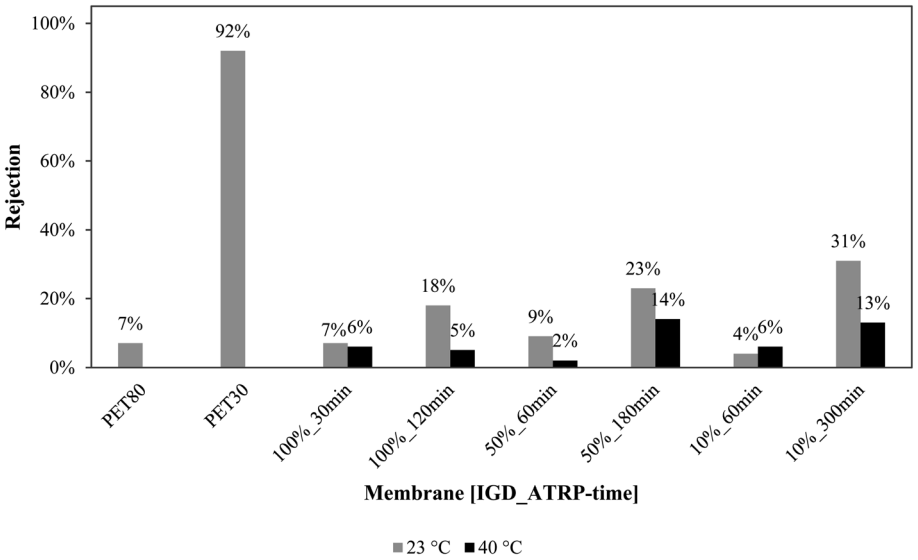

Fig. 7 Rejection data for BSA filtrations through PET80-*g*-PNIPAAm membranes modified with maximum and reduced initiator density (50 and 10%; the relative error of data from repeated experiments was <10%).

pronounced switchability, from 86% at 23 °C to 9% at 45 °C. The discrepancy between estimated pore size at low temperature (68 nm) and observed rejection (86%) is much larger than for the unmodified membrane (35 nm & 22%). This can in parts be due to an underestimation of effective pore size because of the assumptions made for the estimation of hydrodynamic pore diameter (*cf.* Section 3.1); for instance, polydispersity of the grafted layer will lead to larger steric hindrance for passage of particles through the pores by a small fraction of longer than average chains. On the other hand, particle fouling during ultrafiltration (stronger of grafted compared to unmodified membrane and for grafted membranes also stronger at low compared to high temperature, see J/J_0 values in Table 2) could also contribute. For the membranes prepared at lower IGD but almost same polymerization time, leading to lower grafting density (10%_60 min), very similar effects with respect to size-selective sieving and its switchability could be achieved at lower grafting density. This can be related to the higher flexibility of grafted polymer chains in the "mushroom" compared to the "brush" state (*cf.* Scheme 1). In line with the argumentation above the discrepancy between rejection of 20 nm particles and estimated pore size from water flux is also very large. Results for membrane 10%_180 min demonstrate that quantitative rejection at low temperature and significant passage at high temperature can be tuned by SI-ATRP of PNIPAAm.

3.3.2 BSA filtration. The rejection of the model protein BSA having a diameter of 7 nm for selected PET80-*g*-PNIPAAm membranes with different grafting density and chain lengths as well as unmodified membranes as reference is shown in Fig. 6. Rejection for BSA by unmodified PET80 and PET30 membranes at 23 °C was 7 and 92%, respectively. Compared to the results with the 20 nm silica particles on the same membranes (*cf.* Section 3.2.1), the values are considerably higher; this can be related to fouling (J/J_0 values are much lower). Tunability and switchability of rejection due to PNIPAAm grafting can be demonstrated. The effect of grafting density can be seen very clearly when comparing the membranes 100%_120 min and 10%_360 min, which have about the same degree of grafting. The rejection and absolute change of protein passage were larger for the membrane with the lower grafting density in line with its higher chain flexibility (indicated by the higher thermo-responsive switching ratio; *cf.* Table 1, Scheme 1 and Fig. 7).

3.3.3 Ultrafiltration of mixtures of silica nanoparticles and BSA. Finally, the proof of feasibility of a switchable fraction of two different colloids has been attempted. A membrane prepared at low IGD and relatively short polymerization time (10%_60 min) was used because from the single particle ultrafiltration experiments at low temperature an almost quantitative rejection of 20 nm silica and almost no BSA rejection had been found while silica passage was largely increased at high temperature (*cf.* Sections 3.3.1 and 3.3.2). The analysis of the permeate was performed by using DLS, results are shown in Fig. 8. The permeate obtained at 23 °C indeed contained only

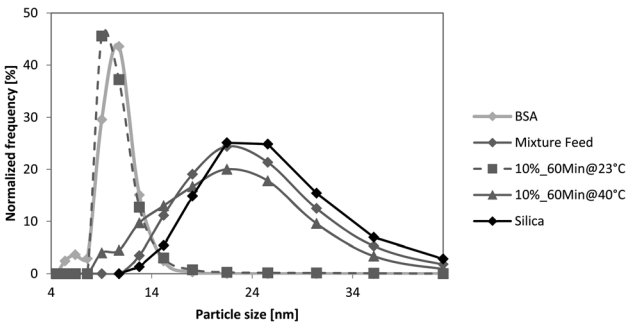

Fig. 8 Particles size distribution measured by DLS, in comparison to references for solutions/dispersions of single components and the mixture used as feed. BSA containing reference and feed samples were stored at the respective temperature according to filtration and waiting times to minimize discrepancies.

BSA (within the limits of this analysis) while at 40 °C both colloids were found in the permeate.

4. Conclusions

The results of this study demonstrate a significant extension of knowledge about the design of polymer-grafted membranes with tunable and switchable barrier pore size, by combination of track-etched membranes with well-defined cylindrical pore structure and controlled surface-initiated graft copolymerization. Conditions for well-controlled SI-ATRP of PNIPAAm on membranes with 35 and 110 nm pore diameter at varied grafting density, tuned by varied ATRP initiator density, were successfully implemented and utilized. Characterization in terms of hydrodynamic pore diameter or effective grafted layer thickness revealed information about the grafted layer architecture, clearly in the "brush" state at high grafting density and sufficient degree of grafting, clearly in the loose "mushroom" state for low grafting density and relatively low degree of grafting. In this context, the switching ratio, *i.e.* the grafted layer thickness in swollen *vs.* collapsed states, can be used as quantitative criterion. Rejection of model proteins and silica particles revealed ultrafiltration properties which are tunable by the initiator density and SI-ATRP conditions and clearly switchable upon temperature change. Discrepancies between pore diameters estimated from water flux measurements and colloid rejections can be interpreted by effects of real grafted structure and architecture (bigger discrepancies for "mushroom" due to larger spacing between polymer chains/higher flexibility compared to "brush") as well as membrane fouling (more pronounced for protein, but also not negligible for silica). Overall, the knowledge about design and synthesis may be used for membranes for controlled release of drugs (proteins) or, by transfer to other base membranes, also for tunable and switchable mass separation in various sectors.

Conflicts of interest

There are no conflicts to declare.

Notes and references

1 *Smart Membranes*, ed. L. Y. Chu, RSC Publishing, 2019, ISBN: 978-1-78801-243-0.
2 D. Wandera, S. R. Wickramasinghe and S. M. Husson, Stimuli-responsive membranes, *J. Membr. Sci.*, 2010, **357**, 6.
3 Q. Yang, N. Adrus, F. Tomicki and M. Ulbricht, Composites of functional polymeric hydrogels and porous membranes, *J. Mater. Chem.*, 2011, **21**, 2783.
4 Z. Liu, W. Wang, R. Xie, X. J. Ju and L. Y. Chu, Stimuli-responsive smart gating membranes, *Chem. Soc. Rev.*, 2016, **45**, 460.
5 H. G. Schild, Poly(N-isopropylacrylamide): experiment, theory and application, *Prog. Polym. Sci.*, 1992, **17**, 163–249.
6 C. A. Naini, S. Franzka, S. Frost, M. Ulbricht and N. Hartmann, Probing the intrinsic switching kinetics of ultrathin thermo-responsive polymer brushes, *Angew. Chem., Int. Ed.*, 2011, **50**, 4513–4516.
7 C. J. Wu, R. Xie, H. B. Wei, T. T. Xu, Z. Liu, W. Wang, X. J. Jua and L. Y. Chu, Fabrication of a thermo-responsive membrane with cross-linked smart gates via a 'grafting-to' method, *RSC Adv.*, 2016, **6**, 45428.
8 A. Saad, R. Mills, H. Wan, M. A. Mottaleb, L. Ormsbee and D. Bhattacharyya, Thermo-responsive adsorption-desorption of perfluoroorganics from water using PNIPAm hydrogels and pore functionalized membranes, *J. Membr. Sci.*, 2020, **599**, 117821.
9 B. P. Tripathi, N. C. Dubey, F. Simon and M. Stamm, Thermo responsive ultrafiltration membranes of grafted poly(N-isopropyl acrylamide) via polydopamine, *RSC Adv.*, 2014, **4**, 34073.
10 R. Nechikkattu and S. Athiyanathil, Thermo-responsive poly(ethylene-co-vinyl alcohol) based asymmetric membranes, *RSC Adv.*, 2016, **6**, 114276.
11 L. J. Zhu, H. M. Song, C. Li, G. Wang, Z. X. Zeng and Q. J. Xue, Surface wormlike morphology control of polysulfone/poly(N-isopropylacrylamide) membranes by tuning the two-stage phase separation and their thermo-responsive permselectivity, *J. Membr. Sci.*, 2018, **555**, 290–298.
12 S. Frost and M. Ulbricht, Thermoresponsive ultrafiltration membranes for the switchable permeation and fractionation of nanoparticles, *J. Membr. Sci.*, 2013, **448**, 1–11.
13 H. Kuroki, H. Ohashi, T. Ito, T. Tamaki and T. Yamaguchi, Isolation and analysis of a grafted polymer onto a straight cylindrical pore in a thermo-responsive gating membrane and elucidation of its permeation behavior, *J. Membr. Sci.*, 2010, **352**, 22–31.
14 A. Friebe and M. Ulbricht, Controlled pore functionalization of poly(ethylene terephthalate) track-etched membranes via surface-initiated atom transfer radical polymerization, *Langmuir*, 2007, **23**, 10316–10322.
15 C. Geismann, A. Yaroshchuk and M. Ulbricht, Permeability and electrokinetic characterization of poly(ethylene terephthalate) capillary pore membranes with grafted temperature-responsive polymers, *Langmuir*, 2007, **23**, 76–83.
16 N. Adrus and M. Ulbricht, Novel hydrogel pore-filled composite membranes with tunable and temperature-responsive size-selectivity, *J. Mater. Chem.*, 2012, **22**, 3088–3098.
17 F. Tomicki, D. Krix, H. Nienhaus and M. Ulbricht, Stimuli-responsive track-etched membranes via surface-initiated controlled radical polymerization: influence of grafting density and pore size, *J. Membr. Sci.*, 2011, **377**, 124–133.
18 P. G. de Gennes, Conformations of polymers attached to an interface, *Macromolecules*, 1980, **13**, 1069–1075.
19 H. Yim, M. S. Kent, S. Mendez, G. P. Lopez, S. Satija and Y. Seo, Effect of grafting density and molecular weight on the temperature-dependent conformational change of poly(N-isopropylacrylamide) grafted chains in water, *Macromolecules*, 2006, **39**, 3420–3426.

20 D. I. Dimitrov, A. Milchev, K. Binder and D. W. Heermann, Structure of polymer brushes in cylindrical tubes: a molecular dynamics simulation, *Macromol. Theory Simul.*, 2006, **15**, 573–583.

21 M. Ciampolini and N. Nardi, Five-coordinated high-spin complexes of bivalent cobalt, nickel and copper with tris(2-dimethylaminoethyl)amine, *Inorg. Chem.*, 1966, **5**, 41–44.

22 J. R. Colvin, Size and shape of lysozyme, *Can. J. Chem.*, 1952, **30**, 831–834.

23 S. Mendez, J. G. Curro, J. D. McCoy and G. P. Lopez, Computational modeling of the temperature-induced structural changes of tethered poly(N-isopropylacrylamide) with self-consistent field theory, *Macromolecules*, 2005, **38**, 174–181.

24 J. B. Kim, M. L. Bruening and G. L. Baker, Surface-initiated atom transfer radical polymerization on gold at ambient temperature, *J. Am. Chem. Soc.*, 2000, **122**, 7616–7617.

25 Z. Bao, M. L. Bruening and G. L. Baker, Control of the density of polymer brushes prepared by surface-initiated atom transfer radical polymerization, *Macromolecules*, 2006, **39**, 5251–5258.

26 B. Jachimska, M. Wasilewska and Z. Adamczyk, Characterization of globular protein solutions by dynamic light scattering, electrophoretic mobility, and viscosity measurements, *Langmuir*, 2008, **24**, 6866–6872.

27 S. C. Chen, D. Segets, T. Y. Ling, W. Peukert and D. Y. H. Pui, An experimental study of ultrafiltration for sub-10 nm quantum dots and sub-150 nm nanoparticles through PTFE membrane and nuclepore filters, *J. Membr. Sci.*, 2016, **497**, 153–161.

28 H. Lee, D. Segets, S. Süß, W. Peukert, S. C. Chen and D. Y. H. Pui, Liquid filtration of nanoparticles through track-etched membrane filters under unfavorable and different ionic strength conditions: experiments and modeling, *J. Membr. Sci.*, 2017, **524**, 682–690.

